Bilayer Phosphorene Under High Pressure: *In Situ* Raman Spectroscopy

Journal:	*Physical Chemistry Chemical Physics*
Manuscript ID	CP-ART-02-2019-000816.R1
Article Type:	Paper
Date Submitted by the Author:	02-Mar-2019
Complete List of Authors:	Akhtar, Meysam; University of Louisville, Department of Physics and Astronomy Zhang, Congyan; University of Louisville, Physics and Astronomy Rajapakse, Manthila; University of Louisville, Department of Physics and Astronomy Musa, Rajib; University of Louisville, Department of Physics and Astronomy Yu, Ming; University of Louisville, Department of Physics and Astronomy Sumanasekera, Gamini; University of Louisville, Physics Jasinski, Jacek; Universiyty of Louisville, Conn Center for Renewable Energy Research

PCCP

ARTICLE

Bilayer Phosphorene Under High Pressure: *In Situ* Raman Spectroscopy

Received 00th January 20xx,
Accepted 00th January 20xx

DOI: 10.1039/x0xx00000x

www.rsc.org/

Meysam Akhtar,[a] Congyan Zhang,[a] Manthila Rajapakse,[a] Rajib Musa,[a] Ming Yu,[a] Gamini Sumanasekera [a,b] and Jacek B. Jasinski *[b]

In this study, bilayer phosphorene samples were subjected to high pressure using a Diamond Anvil Cell (DAC) and their vibrational properties were studied via *in situ* Raman spectroscopy. Systematic shifting in the Raman frequency of A_g^1, B_{2g}, and A_g^2 modes was observed and theoretical calculations were performed to understand the relationship between the strain and the vibrational properties. The changes in the vibration modes under the pressure are found to reflect the deformations in the structure and its stiffness. Firstly, the study shows a substantial pressure-induced enhancement of the interactions between atoms for the out-plane mode A_g^1, mainly due to the directional nature of the lone pair of electrons and charge transfer. However, these interactions and observed blue shift of the A_g^1 Raman peak are much weaker than those in bulk black phosphorous. Secondly, while a significant enhancement of the atomic interactions due to bond length change is also observed for the in-plane mode B_{2g} along the zigzag direction, there is almost negligible effect on the in-plane mode A_g^2 along the armchair direction. The results add to the knowledge on mechanical properties and strain engineering in phosphorene towards novel functionalities and applications of this intriguing two-dimensional (2D) material.

Introduction

Phosphorene, a novel two-dimensional (2D) material, is gaining researchers' attention due to its exceptional properties, including unique layer structure, widely tunable band gap, strong in-plane anisotropy, and high carrier mobility[1]. Unlike graphene and most other 2D materials, phosphorene does not form atomically flat sheets but has a puckered honeycomb structure[2], due to its sp^3 hybridization of atoms[3]. The electronic bandgap of phosphorene varies from 0.3 eV for bulk material[4, 5] to ~2 eV for a monolayer[6] and such a strong dependence on the number of layers originates from the loss of interlayer hybridization in few layer systems[7]. The highly tunable band gap along with other key characteristics such as high carrier mobility (~300 $cm^2V^{-1}s^{-1}$) and strong in-plane anisotropy, particularly the anisotropy of electric conductance[8], make phosphorene a highly promising material for both nano- and optoelectronic applications. Interestingly, the on/off ratio in field effect transistor (FET) devices and the carrier mobility are also layer-dependent[7]. Applications of phosphorene range from energy conversion/storage to thermoelectrics, to optoelectronic and spintronics and to sensors and actuators. Its compatibility with other 2D materials in so-called van der Waals heterostructures can offer solutions for important issues, such as surface degradation, doping, or control of surface/interface electronic structure. Additionally, properties and functionalities of phosphorene can be also tuned by external stimuli such electric fields or strains. In fact, several recent theoretical studies have indicated that strain engineering can be a viable strategy to tune the electronic structure of phosphorene[9-11]. In particular, electronic phase transitions, such as direct-indirect bandgap or metal-insulator transitions have been predicted[12-14]. However, to date, only a little experimental work has been done to corroborate theoretical predictions and enable better understanding of phosphorene under strain conditions. To this end, here, we report our recent studies on vibrational properties of phosphorene under high pressure in a diamond anvil cell (DAC). *In situ* Raman spectroscopy was used to measure the vibrational modes of bilayer phosphorene flakes as a function of pressure and all three main Raman peaks of orthorhombic few-layer phosphorene were found to undergo a blue shift, but with different rates. The experimental results were explained by computational calculations performed using density functional theory (DFT) method. The changes in the vibration frequencies under the high pressure were found to reflect the change in the stiffness of the system associated with the deformation of the structure.

Results and discussion

Dimethylformalhide (DMF) dispersions of phosphorene flakes were obtained by liquid mechanical exfoliation (LME) followed by centrifugation of black phosphorus crystals synthesized by short transport growth method. Synthesis procedure and LME

[a] Department of Physics and Astronomy, University of Louisville, Louisville, KY, 40292, USA.
[b] Conn Center for Renewable Energy Research, University of Louisville, Louisville, KY, 40292, USA. E-mail: jacek.jasinski@louisville.edu; Tel: +1-502 852 6338.
Electronic Supplementary Information (ESI) available: [details of any supplementary information available should be included here]. See DOI: 10.1039/x0xx00000x

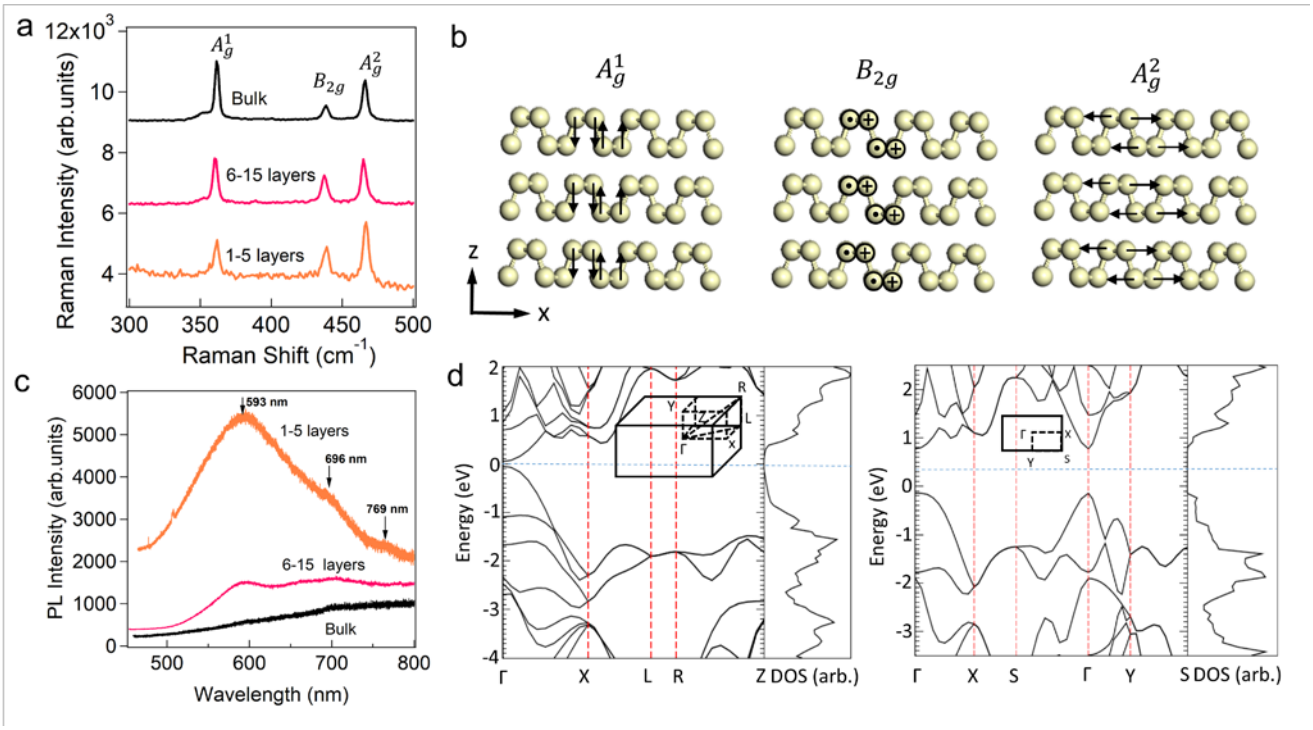

Fig. 1 (a) Raman spectra of bulk black phosphorus and phosphorene samples extracted from upper and lower fraction in centrifuge vial. (b) Schematic showing the three main vibrational modes of phosphorene, where the mode B_{2g} is indicated by crosses (into the page) and dots (out of the page), respectively. (c) PL spectra of bulk black phosphorus and phosphorene from upper and lower fraction in centrifuge vial. (d) Calculated electronic band structure and the densities of states (DOS) of bulk black phosphorus (left) and monolayer phosphorene (right). The inserts are the first Brillouin zones and the Fermi level is indicated by the blue-dashed line.

process are shown schematically under supporting information in Fig. S1a-c and Fig. S2, respectively. Detailed descriptions are provided in the Experimental. Extensive post-fabrication characterization methods were utilized to verify the structure and morphology of these samples. Scanning electron microscopy (SEM) and atomic force microscopy (AFM) confirmed that the samples obtained after centrifugation consists of flakes in micrometer size (Fig. S3a-b). The flake morphology was also confirmed by transmission electron microscopy (TEM) (Fig. S3c-d) and scanning TEM (STEM) (Fig. S4a). In addition, electron diffraction of the flakes produced single crystal patterns with d-spacing values consistent with the structure of phosphorene. For the pattern shown in inset of Fig. S3c, d-spacing values were measured at 0.26 nm, 0.16 nm, and 0.17 nm for planes (111), (200), and (022), respectively. Previous studies found 0.26 nm for the (111) plane and 0.19 nm for (022) plane[15-18]. Energy dispersive x-ray spectroscopy (EDS) verified that phosphorus was the main chemical element of the flakes (Fig S4). There were also trace amounts of carbon and oxygen but they could be attributed to both environmental effects and potential doping from the DMF.

Raman spectra of phosphorene samples acquired from the top and bottom fractions (corresponding to 1-5 and 6-15 layers, respectively, as determined from photoluminescence (PL) measurements) of centrifuged samples are compared with the spectrum of bulk black phosphorus in Fig. 1a. Main vibrational modes of phosphorene include the A_g^1 (out-of-plane), B_{2g} (in-plane along the zigzag direction), and A_g^2 (in-plane along the armchair direction) modes, which are shown schematically in Fig. 1b. The corresponding Raman peaks are located at 360 cm^{-1}, 440 cm^{-1}, and 468 cm^{-1}, respectively[19-22]. Fig. 1c shows the PL spectra of bulk black phosphorus and phosphorene samples taken from the top and bottom of the sample after centrifugation. As expected, bulk black phosphorus does not show any peaks in the region of interest due to its small band gap in the infrared region with a value of E_g = 0.3 eV[4, 5]. On the other hand, phosphorene samples of the top fraction show a very strong peak at 593.2 nm (2.09 eV) and weaker peaks at 696.0 nm (1.78 eV) and 769.0 nm (1.61 eV), following the finite layer thickness distribution (1-5 layers). The strongest peak at 2.09 eV, is suspected to be due to monolayer phosphorene as its value is close to the recently reported monolayer experimental value of 2.26 eV[23]. Energy band gaps of 1.6 eV[24] and 1.29 eV[25] have been reported for bilayer phosphorene from PL estimates, whereas a value 2 eV has been calculated for monolayer phosphorene[6]. Fig. 1d shows the calculated electronic band structures and densities of states for black phosphorus (left panel) and black phosphorene (right panel) using density functional theory (DFT)[26, 27]-based Vienna Ab-initio Simulation Package (VASP)[28]. Calculated band gap is 0.17 eV for black phosphorus and 0.91 eV for black phosphorene, respectively. The underestimated band gaps compared to the

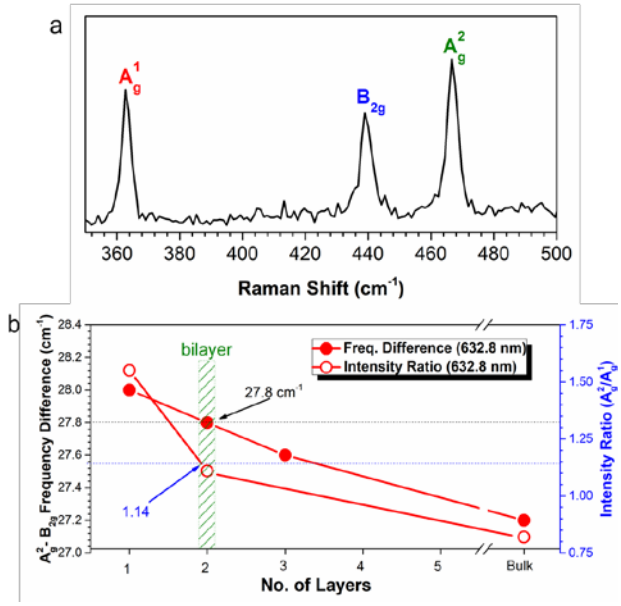

Fig. 2 (a) Room temperature, ambient pressure spectrum of bilayer phosphorene sample. (b) The intensity ratio of A_g^2/A_g^1 and the Raman shift difference A_g^2-B_{2g} vs. number of layers for red laser excitation (after Ref.[26]) which was used for the number of layer calibration (red points). By comparing this data with our experimental results, bilayer phosphorene flake morphology was determined for the sample.

experimental values is mainly due to the self-interaction error in DFT calculations.

For subsequent *in situ* high-pressure study, bilayer phosphorene flakes were identified and selected based on room temperature, ambient pressure Raman spectra, as the one shown in Fig. 2a. The intensity ratio between A_g^2 and A_g^1 peaks as well as the Raman shift difference between A_g^2 and B_{2g} peaks are key parameters for determining the number of layers of a phosphorene sample. For the spectrum shown in Fig. 2a, the intensity ratio of A_g^2/A_g^1 was found to be 1.14 and the Raman shift difference A_g^2-B_{2g} was found to be 27.8 cm^{-1}. Comparing these values with the literature data[29] indicates that this was a bilayer flake (see Fig. 2b).

A schematic of experimental setup used for *in situ* high-pressure Raman measurements is shown in Fig. 3a and description of experimental details is provided in the Experimental. Raman spectra measured for the bilayer sample at pressure from 0 GPa to ~10 GPa are shown in Fig. 3b. Inducing pressure in phosphorene results in an increase in the Raman shifts similar to other layered materials[29-33]. Such behaviour is also apparent in the data shown in Fig. 3c. The observed changes in the Raman shifts are different for different vibrational modes and they all follow the quadratic behaviour. The fitted quadratic functions are also shown in Fig. 3c and the obtained fitting parameters are provided in Supporting Information. The linear function fitting of the initial slopes, for the pressures of up to 5 GPa (Supporting Information), yields the highest pressure coefficients for the A_g^1 mode. The corresponding value measured for the bilayer sample is 1.47±0.05 cm^{-1}/GPa. On the other hand, the coefficients measured for the B_{2g} and A_g^2 modes are significantly smaller. Their corresponding values are 0.50±0.05 cm^{-1}/GPa and 0.22±0.02 cm^{-1}/GPa, respectively. Similar trends are obtained from the pressure coefficients obtained as derivatives of the

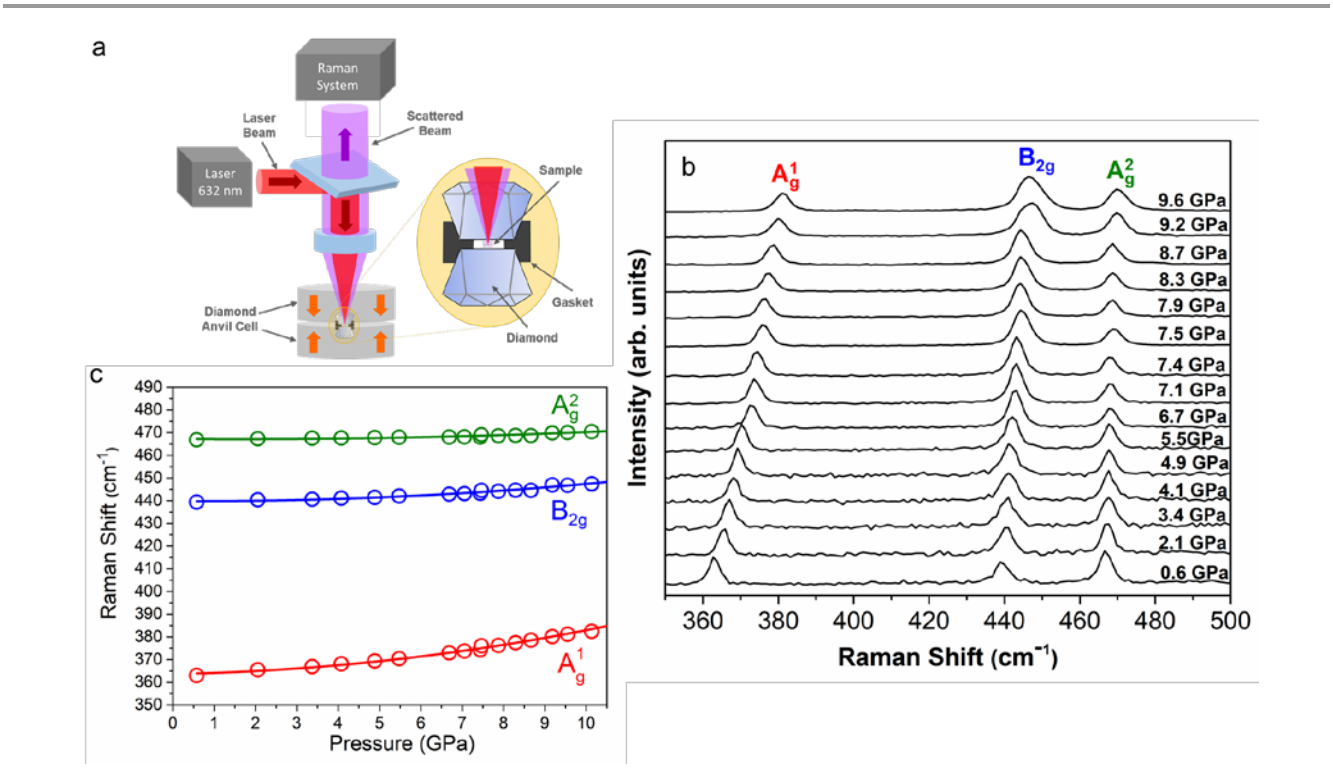

Fig. 3 (a) Schematic of experimental setup used for *in situ* high-pressure Raman spectroscopy. (b) High-pressure evolution of Raman spectra and (c) the Raman shifts with quadratic fits of bilayer phosphorene sample.

Raman shift vs. pressure data (Table S1). Upon decompression, the spectroscopic changes are reversible and the high-pressure phase reverts to the original structure.

In order to explain the observed experimental evolution of vibrational modes, theoretical calculations and modelling for black phosphorous were performed using the density functional theory (DFT) [26, 27] framework, as described in the Experimental. There are nine vibration modes (B_{2u}, A_g^2, B_{2g}, A_u, $B_{3g(2)}$, A_g^1, $B_{3g(1)}$, B_{1g}, B_{1u}) and only six are Raman-active modes (A_g^2, B_{2g}, $B_{3g(2)}$, A_g^1, $B_{3g(1)}$, B_{1g})[34, 35]. Typically, measured Raman spectrum of an exfoliated black phosphorus includes A_g^2, B_{2g}, and A_g^1, respectively. The pressure is estimated by $P \approx \Delta E / A \Delta b$. Calculated vibration frequencies at Γ point for these three main vibration modes under high pressure (stars in Fig. 4a) are compared with experimental Raman data for bilayer phosphorene (open circles in Fig. 4a). Very interesting finding is that both the out-of-plane vibration mode A_g^1 and the in-plane vibration mode B_{2g} along the zigzag direction increases almost proportionally, at least for lower pressures, while the in-plane vibration mode A_g^2 along the armchair direction show nearly unchanged under the high pressure, in agreement with our experimental observations (see Fig. 4a).

The changes in the vibration frequencies under the pressure reflect the change in the stiffness of the system associated with the deformation of the structure. Such structural deformation can be analysed in terms of the bond lengths and the bond angles, as illustrated in Fig. 4b-c for black phosphorus. Apparently, both bond angles α and β are reduced under the uniform compression. Interestingly, the reduction of these angles mainly shortens the bond length b_1 but not b_2. In fact, b_2 even slightly increases. We note that simultaneously, there is a big decrease in the interlayer distance d. The combination of the increasing in b_2 along z-direction (i.e., b_{2z}) and the decreasing in d under pressure demonstrates that the compression (or the pressure)-induced charge redistribution due to the directional nature of lone pair of electrons leads to an enhancement of the interaction between interlayer atoms, and then, stores more energy in the system with an increase of the stiffness which leads to an increase in the vibration frequency of the out-plane mode A_g^1. However, such effect on bilayer is weakened (compared to bulk and multilayer phosphorene) due to weakened interlayer interactions. Further analysis also showed that the change in the bond b_1 is mainly due to the shortness along the y-direction (i.e., b_{1y}), which strengthens the interaction between atoms along zigzag direction, and

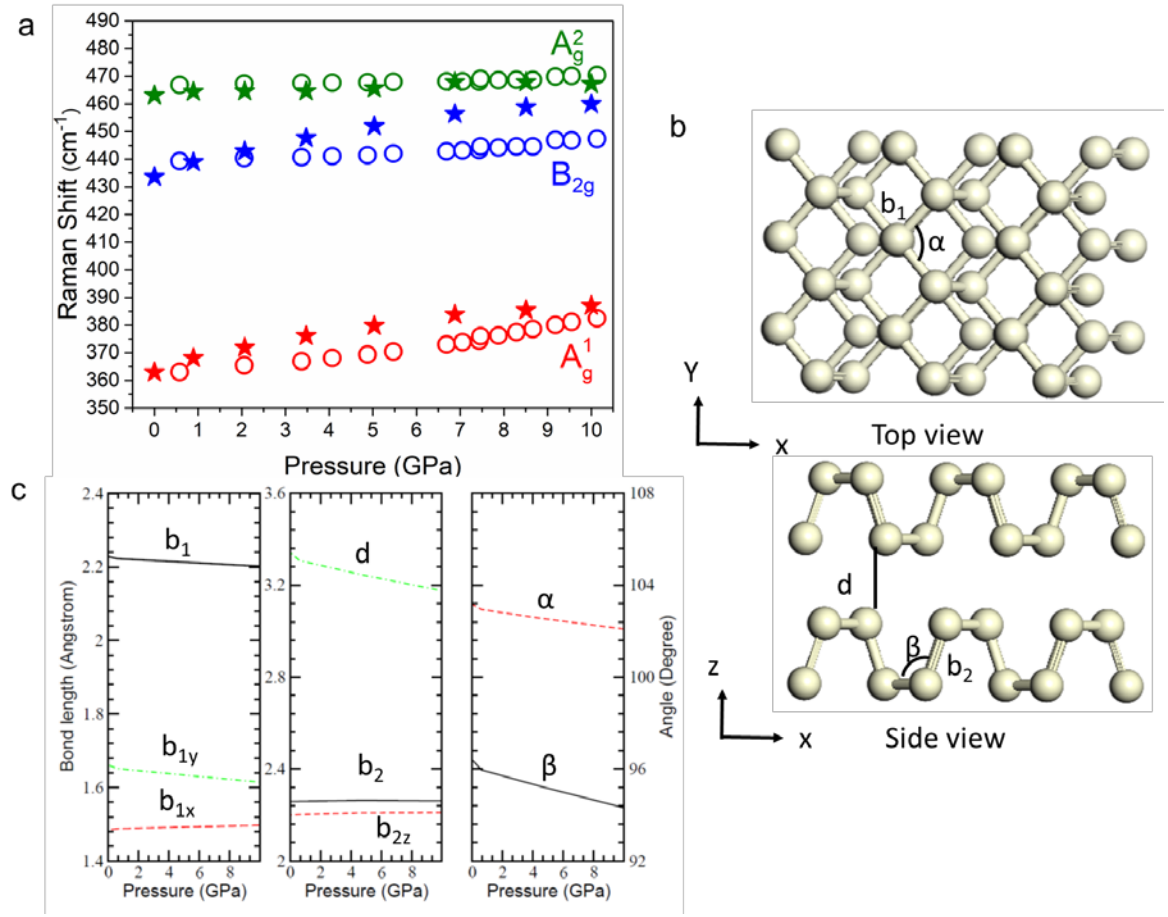

Fig. 4 (a) Comparison of high-pressure experimental (open circles) and theoretical (stars) Raman shift for the three main modes. (c) The pressure dependences of the bond lengths b_1, b_2, their components, the angles α, and β. These structural parameters are defined in (b).

therefore enhances the vibration frequency of the in-plane mode B_{2g}.

Experimental

Synthesis of Black Phosphorous

Black phosphorus crystals were synthesized using a short transport growth method[36]. A quartz glass ampule was filled with 24 mg of tin (Sn), 12 mg of tin iodide (SnI4), and 500 mg of red phosphorus, in that order. The ampule was then evacuated down to 10^{-6} Torr and sealed afterward using an oxy-acetylene flame torch. Growth of bulk black phosphorus was done in a single zone quartz tube furnace following the heating profile shown in Fig. S1c. At high temperature, the furnace had a temperature gradient of about 50 °C and the end of the glass tube that contained the precursor material was placed in the hotter end. After the process, when the ampoule reached room temperature, large crystals of black phosphorus were formed.

Liquid Mechanical Exfoliation

DMF-based suspension of black phosphorus powder was sonicated for 90 minutes. The suspension was prepared in an ambient argon environment and DMF was used as the medium in order to prevent material degradation. Stability is a main concern because of phosphorene reactivity due to each phosphorus atom in the system having a lone electron pair ready for bonding purposes. The sonication produced phosphorene flakes with thickness in the range of 1-15 atomic layers, as measured by PL. The flakes were separated into fractions by subsequent centrifugation at 10,000 rpm for 30 minutes at 25 °C. During centrifugation, the fraction of thicker flakes (6-15 layers) sedimented at the bottom of the vial, while thinner ones (1-5 layers) remained in the suspension.

Characterization of Phosphorene Samples

TEM specimens are prepared by suspending a lacey carbon-coated TEM grid into the dimethlyformalhide/phosphorene dispersion obtained after LME. As the grid was slowly pulled out of the mixture, it was able to catch several flakes. Once the grid/phosphorene system had dried, it was placed inside FEI Tecnai F20 transmission electron microscope, equipped with EDAX spectrometer, for the TEM, STEM, electron diffraction, and EDS analysis. The additional microscopic characterization was done with the use of FEI Nova 600 SEM and Asylum MF3D Conductive AFM.

Raman spectra were calibrated to Si 520 cm^{-1} peak. For Raman, the excitation laser wavelength was 632 nm at 10% laser power and exposure time was 15 sec with numerous accumulations to slow degradation of samples. Previous studies have found that the intensity of the A^1_g peak in relation to the Si peak can be used to determine the number of layers of phosphorene [24]. Based on the above intensity ratio calibration, the current work's Raman spectrums show between 3 and 9 layers. The same experimental system was used to measure PL spectra however, the measurements done using 442 nm wavelength excitation laser at 10% and 30 second exposure time.

High-Pressure Experiments

In situ high-pressure Raman measurements were conducted at room temperature using the diamond anvil cell. The high-pressure evolution of Raman frequency of phosphorene (few-layer black phosphorus) from ambient pressure to ~10 GPa was collected at room temperature. High pressure was generated by a gas membrane-driven diamond anvil cell (Diacell® HeliosDAC Almax easyLab) equipped with 800 µm culet diamonds. Inconel gasket with 10 mm in diameter and 0.20 mm thickness were pre-indented down to 0.05 mm. Micro Electrical discharge machining (EDM) (Hylozoic Products) was used for drilling a small hole (0.3 mm in diameter) for sample loading. Each sample was excited with He-Ne (633 nm) red laser in a 180° backscattering geometry using a Leica microscope with a 50X Nikon objective lens (T Plan EPI SLWD, Working Distance = 22 mm). Renishaw inVia spectrometer with an 1800 lines per millimeter grating, a charge-coupled device (CCD) detector, and effective resolution of 0.5 cm^{-1} was used for Raman spectroscopy. The Raman spectra were collected at various pressures during compression and decompression. Ruby fluorescence R_2-line shifts were used for pressure calibration. This method is known to have an error of ± 5%. The ruby fluorescence was measured with same Renishaw spectrometer and He-Cd (442 nm) blue laser (IK series, Kimmon Koha Co.) during compression and decompression. The pressure of gas membrane (which drive the piston of the cell) was calibrated against the pressure inside the DAC. For each high-pressure experiment, small pieces of phosphorene samples were loaded into the gasket hole under an optical microscope (AmScope Trinocular Stereo Zoom) with long working distance objective lenses. It was visually ensured that the phosphorene samples were floating in the middle of the hole and were not in contact with the gasket or the diamond. We tested two solutions Methanol:Ethanol:DI-water (16:4:1) and Dimethylformamide (DMF) separately as the quasi-hydrostatic pressure media[37-39].

Computational Methods

The overall computational calculations in this study was mainly carried out by employing the DFT[26, 27] framework, as implemented in the VASP[28]. The electron-ion interactions were described by the Projector Augmented Wave (PAW)[40], while electron exchange-correlation interactions were treated by the generalized gradient approximation (GGA)[41] in the scheme of Perdew Burke Ernzerhof (PBE)[42]. The structural relaxation was performed using Congregate-Gradient algorithm [43] implemented in VASP. An energy cutoff was set to be 500 eV for the plane wave basis in all calculations, and the criteria for the convergences of energy and force in relaxation processes were set to be 10-5 eV and 10-4 eV/Å, respectively. A 1x1 primitive cell contains 4 phosphorus atoms was chosen to study the behavior of black phosphorus under certain pressure. The Brillouin zones (BZ) were sampled by 9 × 9 × 9 k-point meshes generated in accordance with the Monkhorst-Pack scheme [44] in the calculations. The optimized lattice constants for black phosphorus are a = 3.323 Å, and b = 11.085 Å, and c = 4.515 Å which are consistent with the previous DFT results[30, 45-49]. In the processes of investigating the vibration modes of black phosphorus under pressure, a uniform compression was

introduced (see Fig. 3(a)) and a fully relaxation under the compression was performed. The vibration modes at Γ point were calculated from Hessian matrix implemented in VASP code [28].

Conclusions

Bilayer phosphorene samples were obtained using liquid mechanical exfoliation. The experimental and theoretical studies of their vibrational properties under high-pressure were carried out. *In situ* Raman spectra were measured systematically at different pressures from 0 to ~10 GPa to study the pressure evolution of Raman peaks and associated vibrational modes. Simultaneous first principle calculations using density functional theory (DFT) method were also performed and the results were compared with the experiment. The observed changes in the vibration frequencies under the high pressure were found to reflect the change in the stiffness of the system associated with the deformation of the structure. Moreover, while the pressure coefficients of the three fundamental vibrational modes showed relative trends similar to those in bulk black phosphorus, their absolute values were lower due to substantially reduced interlayer interactions.

Conflicts of interest

The authors declare no conflict of interest.

Acknowledgements

This work was supported by the U.S. Department of Energy, Office of Science, Basic Energy Sciences, under Award # DE-SC0019348. The authors would like to thank Dr. George Anderson for his assistance with the fabrication and characterization of phosphorene samples.

Notes and references

1. M. Akhtar, G. Anderson, R. Zhao, A. Alruqi, J. E. Mroczkowska, G. Sumanasekera and J. B. Jasinski, *npj 2D Materials and Applications*, 2017, **1**, 5.
2. A. Castellanos-Gomez, L. Vicarelli, E. Prada, J. O. Island, K. L. Narasimha-Acharya, S. I. Blanter, D. J. Groenendijk, M. Buscema, G. A. Steele, J. V. Alvarez, H. W. Zandbergen, J. J. Palacios and H. S. J. van der Zant, *2D Mater.*, 2014, **1**, 19.
3. A. S. Rodin, A. Carvalho and A. H. Castro Neto, *Physical Review Letters*, 2014, **112**, 176801.
4. D. Warschauer, *Journal of Applied Physics*, 1963, **34**, 1853-1860.
5. Y. Akahama, S. Endo and S. Narita, *Journal of the Physical Society of Japan*, 1983, **52**, 2148-2155.
6. X. Zhang, H. Xie, Z. Liu, C. Tan, Z. Luo, H. Li, J. Lin, L. Sun, W. Chen, Z. Xu, L. Xie, W. Huang and H. Zhang, *Angewandte Chemie International Edition*, 2015, **54**, 3653-3657.
7. H. Liu, A. T. Neal, Z. Zhu, Z. Luo, X. F. Xu, D. Tomanek and P. D. D. Ye, *ACS Nano*, 2014, **8**, 4033-4041.
8. H. Liu, A. T. Neal, Z. Zhu, Z. Luo, X. Xu, D. Tomanek and P. D. Ye, *ACS Nano*, 2014, **8**, 4033-4041.
9. H. Ting, H. Yang and D. Jinming, *Nanotechnology*, 2014, **25**, 455703.
10. Y. Ge, W. Wan, F. Yang and Y. Yao, *New Journal of Physics*, 2015, **17**.
11. R. Fei and L. Yang, *Nano Letters*, 2014, **14**, 2884-2889.
12. A. Manjanath, A. Samanta, T. Pandey and A. K. Singh, *Nanotechnology*, 2015, **26**.
13. X. Peng, Q. Wei and A. Copple, *Physical Review B*, 2014, **90**.
14. W. Ju, T. Li, H. Wang, Y. Yong and J. Sun, *Chemical Physics Letters*, 2015, **622**, 109-114.
15. D. J. Late, *Microporous and Mesoporous Materials*, 2016, **225**, 494-503.
16. P. Masih Das, G. Danda, A. Cupo, W. M. Parkin, L. Liang, N. Kharche, X. Ling, S. Huang, M. S. Dresselhaus, V. Meunier and M. Drndić, *ACS Nano*, 2016, **10**, 5687-5695.
17. J. R. Brent, N. Savjani, E. A. Lewis, S. J. Haigh, D. J. Lewis and P. O'Brien, *Chemical Communications*, 2014, **50**, 13338-13341.
18. L. Yangjin, Y. Jun-Yeong, S. Declan, J. Jeongsu, J. G. S. Elton, J. Hu Young and K. Kwanpyo, *Journal of Physics D: Applied Physics*, 2017, **50**, 084003.
19. S. Zhang, J. Yang, R. Xu, F. Wang, W. Li, M. Ghufran, Y.-W. Zhang, Z. Yu, G. Zhang, Q. Qin and Y. Lu, *ACS Nano*, 2014, **8**, 9590-9596.
20. Z. N. Guo, H. Zhang, S. B. Lu, Z. T. Wang, S. Y. Tang, J. D. Shao, Z. B. Sun, H. H. Xie, H. Y. Wang, X. F. Yu and P. K. Chu, *Advanced Functional Materials*, 2015, **25**, 6996-7002.
21. R. Fei and L. Yang, *Applied Physics Letters*, 2014, **105**, 083120.
22. W. Lu, H. Nan, J. Hong, Y. Chen, C. Zhu, Z. Liang, X. Ma, Z. Ni, C. Jin and Z. Zhang, *Nano Research*, 2014, **7**, 853-859.
23. C. Wang, Q. He, U. Halim, Y. Liu, E. Zhu, Z. Lin, H. Xiao, X. Duan, Z. Feng and R. Cheng, *Nature*, 2018, **555**, 231.
24. A. Castellanos-Gomez, L. Vicarelli, E. Prada, J. O. Island, K. L. Narasimha-Acharya, S. I. Blanter, D. J. Groenendijk, M. Buscema, G. A. Steele, J. V. Alvarez, H. W. Zandbergen, J. J. Palacios and H. S. J. van der Zant, *2D Materials*, 2014, **1**.
25. L. Li, Y. Yu, G. J. Ye, Q. Ge, X. Ou, H. Wu, D. Feng, X. H. Chen and Y. Zhang, *Nat Nano*, 2014, **9**, 372-377.
26. W. Kohn and L. J. Sham, *Physical review*, 1965, **140**, A1133.
27. P. Hohenberg and W. Kohn, *Physical review*, 1964, **136**, B864.
28. G. Kresse and J. Furthmüller, *Physical review B*, 1996, **54**, 11169.
29. S. Taizo, K. Kensuke, A. Yuichi, N. Satoshi and T. Takashi, *Japanese Journal of Applied Physics*, 2017, **56**, 05FB06.
30. R. Fei and L. Yang, *Applied Physics Letters*, 2014, **105**.
31. Y. Yan, F. Li, Y. Gong, M. Yao, X. Huang, X. Fu, B. Han, Q. Zhou and T. Cui, *The Journal of Physical Chemistry C*, 2016, **120**, 24992-24998.
32. S. Sugai and T. Ueda, *Physical Review B*, 1982, **26**, 6554-6558.
33. Y. A. Sorb, N. Subramanian and T. R. Ravindran, *Journal of Physics: Condensed Matter*, 2013, **25**, 155401.
34. J. Ribeiro-Soares, R. M. Almeida, L. G. Cançado, M. S. Dresselhaus and A. Jorio, *Physical Review B*, 2015, **91**, 205421.
35. H. B. Ribeiro, M. A. Pimenta and C. J. de Matos, *Journal of Raman Spectroscopy*, 2018, **49**, 76-90.
36. M. Koepf, N. Eckstein, D. Pfister, C. Grotz, I. Krueger, M. Greiwe, T. Hansen, H. Kohlmann and T. Nilges, *Journal of Crystal Growth*, 2014, **405**, 6-10.
37. S. Klotz, J. Chervin, P. Munsch and G. Le Marchand, *Journal of Physics D: Applied Physics*, 2009, **42**, 075413.
38. D. Errandonea, *Physica B*, 2005, **355**, 116.
39. J. Navarro-Sánchez, I. Mullor-Ruíz, C. Popescu, D. Santamaría-Pérez, A. Segura, D. Errandonea, J. González-Platas and C. Martí-Gastaldo, *Dalton Transactions*, 2018, **47**, 10654-10659.
40. P. E. Blöchl, *Physical Review B*, 1994, **50**, 17953.

41. J. P. Perdew, J. A. Chevary, S. H. Vosko, K. A. Jackson, M. R. Pederson, D. J. Singh and C. Fiolhais, *Physical Review B*, 1992, **46**, 6671.
42. J. P. Perdew, K. Burke and M. Ernzerhof, *Physical review letters*, 1996, **77**, 3865.
43. X. Gonze, *Physical Review B*, 1997, **55**, 10337.
44. H. J. Monkhorst and J. D. Pack, *Physical review B*, 1976, **13**, 5188.
45. C. D. Zhang, J. C. Lian, W. Yi, Y. H. Jiang, L. W. Liu, H. Hu, W. D. Xiao, S. X. Du, L. L. Sun and H. J. Gao, *The Journal of Physical Chemistry C*, 2009, **113**, 18823-18826.
46. J. Dai and X. C. Zeng, *Journal of Physical Chemistry Letters*, 2014, **5**, 1289-1293.
47. Y. Du, C. Ouyang, S. Shi and M. Lei, *Journal of Applied Physics*, 2010, **107**, 093718.
48. Y. Takao, H. Asahina and A. Morita, *Journal of the Physical Society of Japan*, 1981, **50**, 3362-3369.
49. L. Cartz, S. Srinivasa, R. Riedner, J. Jorgensen and T. Worlton, *The Journal of Chemical Physics*, 1979, **71**, 1718-1721.